Metal Interactions with a GAAA RNA Tetraloop Characterized by ^{31}P NMR and Phosphorothioate Substitutions†

Melissa Maderia, Thomas E. Horton, and Victoria J. DeRose*

Department of Chemistry, Texas A&M University, College Station, Texas 77842-3012

Received January 21, 2000; Revised Manuscript Received May 1, 2000

ABSTRACT: A metal site in a 5′-GAAA-3′ tetraloop, a stabilizing and phylogenetically conserved RNA motif, is explored using ^{31}P NMR spectroscopy and phosphorothioate modifications. Similar to previous reports [Legault, P., and Pardi, A. (1994) *J. Magn. Reson., Ser. B 103*, 82−86], the ^{31}P NMR spectrum of a 12-nucleotide stem−loop sequence 5′-GG**C**CGAAAG**G**CC-3′ exhibits resolved features from each of the phosphodiester linkages. Titration with Mg^{2+} results in distinct shifts of a subset of these ^{31}P features, which are assigned to phosphodiesters 5′ to A6, A7, and G5. Titration with $Co(NH_3)_6^{3+}$ causes only a slight upfield shift in the A6 feature, suggesting that changes caused by Mg^{2+} are due to inner-sphere metal−phosphate coordination. R_p-Phosphorothioate substitutions introduced enzymatically 5′ to each of the three A residues of the tetraloop provide well-resolved ^{31}P NMR features that are observed to shift in the presence of Cd^{2+} but not Mg^{2+}, again consistent with a metal−phosphate site. Analysis of ^{31}P NMR spectra using the sequence 5′-GG**G**CGAAAG**U**CC-3′ with single phosphorothioate substitutions in the loop region, separated into R_p and S_p diastereomers, provides evidence for an inner-sphere interaction with the phosphate 5′ to A7 but outer-sphere or structural effects that cause perturbations 5′ to A6. Introduction of an R_p-phosphorothioate 5′ to A7 results in a distinct ^{31}P NMR spectrum, consistent with thermodynamic studies reported in the accompanying paper that indicate a unique structure caused by this substitution. On the basis of these results and existing structural information, a metal site in the 5′-GAAA-3′ tetraloop is modeled using restrained molecular dynamics simulations.

5′-UNCG-3′ and 5′-GNRA-3′ (*N* = any nucleotide, R = purine) loop sequences are members of the family of tetraloops that occur frequently in large RNAs such as ribosomal RNA and the group I/group II intron ribozymes (*1*, *2*) and are unusually stabilizing in RNA hairpins (*3*). These tetraloops are predicted to stabilize local structures (*4*−*6*) and initiate folding events (*7*) in structured RNAs, as well as provide for intra- and intermolecular interactions in both RNA (*8*−*13*) and RNA−protein complexes (*14*−*18*). In large RNA molecules, GNRA tetraloops have been shown to dock into RNA tetraloop "receptors" which may be far removed in sequence or present in a different RNA molecule (*8*, *12*, *19*−*20*). The 5′-GAGA-3′ tetraloop also is a target of the protein ricin, which cleaves the first 5′-A in the loop (*14*, *15*, *21*, *22*).

Several GNRA tetraloops have been structurally characterized by either solution NMR[1] (*21*−*27*) or X-ray crystallography (*8*, *12*, *17*, *28*−*32*). Defining characteristics of the stable GNRA tetraloop include a turn between the first and second bases in the loop and unusual G−A hydrogen bonding between the first and fourth bases. These structural features allow stacking between bases in the loop, which in addition to a network of hydrogen bonds are thought to be the basis of enhanced stabilization in this motif.

The 5′-GAAA-3′ (GA_3) tetraloop is a common GNRA sequence and has been structurally and thermodynamically characterized (*5*, *6*, *12*, *24*−*28*). One such tetraloop caps stem II in a commonly used sequence of the hammerhead ribozyme, originally crystallized by Pley and co-workers (*12*, *28*). Legault and Pardi have shown that the GA_3 tetraloop, both in a 12-nucleotide model and within the hammerhead ribozyme, exhibits distinctive ^{31}P chemical shifts (*33*). Recently, Mn^{2+}-dependent broadening of a ^{31}P feature from the hammerhead tetraloop has been reported, indicative of a metal interaction with that tetraloop (*34*). In the course of experiments involving ^{31}P NMR of phosphorothioate-substituted hammerhead ribozyme samples, we also observed evidence for a Cd^{2+} interaction with a phosphorothioate substitution 5′ to an A of the stem II tetraloop (*35*). A recent ^{1}H NMR study by Rüdisser and Tinoco provides evidence for a metal site in a GA_3 tetraloop, for which the authors suggest direct coordination with a phosphate (*36*). These observations suggest a metal site in the tetraloop that can be investigated more thoroughly.

Phosphorothioate substitutions have been used extensively in activity assays as a method of predicting metal−phos-

† This work was supported by the NSF (CAREER), the NIH (GM58096), the Robert A. Welch Foundation, and the Texas Higher Education Coordinating Board Advanced Research Program. V.J.D. is a Cottrell Scholar of the Research Corporation.

* Corresponding author. Phone: 979-862-1401. Fax: 979-845-4719. E-mail: derose@mail.chem.tamu.edu.

[1] Abbreviations: NMR, nuclear magnetic resonance; R_p, a sulfur substitution in the *pro-R* position of a phosphodiester; S_p, a sulfur substitution in the *pro-S* position of a phosphodiester; TEA, triethanolamine; ATP, adenosine 5′-triphosphate; ATPαS, adenosine 5′-*O*-(1-thiotriphosphate); TMP, trimethyl phosphate; GTP, guanosine triphosphate; WT, wild type or an all-phosphodiester backbone with no sulfur modifications; t_m, melting temperature; GRASP, graphical representation and analysis of structural properties (a computer visualization and analysis program); NOE, nuclear Overhauser effect.

10.1021/bi000140l CCC: $19.00
Published on Web 06/22/2000

phodiester interactions (*37*−*48*). In these studies, a decrease in Mg^{2+}-dependent activity and the ability of more thiophilic metals such as Mn^{2+} or Cd^{2+} to "rescue" activity are measured and considered an indicator of metal binding at the phosphorothioate-substituted site. An additional property of phosphorothioate-substituted nucleic acids is the 40−60 ppm downfield shift in the ^{31}P NMR features from the phosphorothioate-substituted sites (*49*−*52*), removing them from the spectrally crowded region of phosphodiesters in large RNA molecules. The substituted sites can be selectively monitored by NMR and probed with combinations of Mg^{2+} and Cd^{2+} to discern the effects of metal binding.

Here, metal−tetraloop interactions are investigated in two 12-nucleotide tetraloop models with the sequences 5′-GG**C**CGAAAG**G**CC-3′ and 5′-GG**G**CGAAAG**U**CC-3′. Native (WT) samples and samples containing multiple and single phosphorothioate substitutions are used in order to take advantage of "metal-switch" Mg^{2+}/Cd^{2+} experiments that help to discern the site and character of metal interactions. Evidence is presented for a metal site localized to one side of the tetraloop and consisting of at least partial inner-sphere binding to the phosphate 5′ to A7 in these sequences, creating perturbations to phosphates 5′ to A6 and G5.

MATERIALS AND METHODS

RNA Synthesis and Purification. The sequences 5′-GG**C**CGAAAG**G**CC-3′ and 5′-GG**G**CGAAAG**U**CC-3′ were used in this study. Unmodified sequences were synthesized via enzymatic transcription using T7 RNA polymerase (*53*, *54*). RNA was purified on 20% or 30% polyacrylamide gels, electroeluted, and extensively dialyzed against 5 mM triethanolamine (TEA) and 100 mM NaCl, pH 7.8, for at least 72 h with five reservoir changes (*54*). The RNA was concentrated (Centricon-3, Amicon), ethanol-precipitated, dried, and resuspended in 5 mM TEA and 100 mM NaCl, pH 7.8. RNA concentrations were determined using calculated extinction coefficients at 260 nm (*55*).

The 12-nucleotide sequences with phosphorothioate modifications 5′ to each adenosine were synthesized via enzymatic transcription using ATPαS in place of ATP (*56*). The RNA was then gel-purified and dialyzed as above. ATPαS was synthesized by standard procedures adapted from previous reports (*50*, *51*, *57*), analyzed for purity on a Vydac Nucleotide column (303NT405), purified of divalent metals on a Chelex-100 (Bio-Rad) exchange column, and exchanged to a Na^+ counterion using Dowex-50-WX8-400 (Sigma).

RNA sequences with single phosphorothioate modifications were purchased (Dharmacon Research, Boulder, CO) as diastereomeric mixtures. The R_p and S_p isomers were separated by reverse-phase C-18 (Pharmacia) HPLC essentially as previously reported (*38*), with the R_p isomer eluting earlier in the gradient. Isomers were verified by treatment with snake venom phosphodiesterase, which cleaves the R_p and not the S_p diastereomer (*38*). After separation of the isomers, the RNA was dialyzed as described above.

^{31}P NMR Spectroscopy. ^{31}P NMR spectra of RNA samples with individual phosphorothioate modifications were recorded at 202 MHz on a Varian Unity spectrometer with a 5 mM broad-band probe, with RNA concentrations of 0.15−0.2 mM. Other ^{31}P NMR spectra were collected at 121 MHz on a Varian Unity Plus instrument with a 5 mM quad probe, with RNA concentrations of 0.5−1.6 mM. T_1 measurements of an RNA with a single phosphorothioate substitution and a 5′-triphosphate gave $T_1 \leq 2$ s. All ^{31}P NMR spectra were run with a 30° pulse applied at a 0.4 s acquisition time. For all spectra recorded at 121 MHz, an internal coaxial tube containing trimethyl phosphate (TMP) in D_2O was used as a reference and set to 3.7 ppm. For all spectra recorded at 202 MHz, samples were run in a Shegemi D_2O matched quartz tube with an external reference of TMP, set to 3.7 ppm. All spectra were recorded in 5 mM TEA and 0.1 M NaCl, pH 7.8, at room temperature. Initial ^{31}P NMR spectra in the absence of added metals were recorded after the sample was heated to 90 °C for 1.5 min, followed by slow cooling. For metal titrations, M^{2+} was added directly to the sample tube from concentrated stock solutions in water, with no additional annealing step. No changes in pH were observed during addition of metals to the buffered solutions.

Determination of the Equilibrium Dissociation Constant. The data were fit (KaleidaGraph, Abelbeck) to eq 1 (*58*) using a simple 1:1 binding model to solve for the equilibrium dissociation constant (K_d) and the total shift for a fully bound RNA−M^{2+} complex ($[\Delta]_T$). In eq 1, $[RNA]_T$ and M are the

$$\Delta_{obs} = \frac{[\Delta]_T}{2[RNA]_T}[(M + [RNA]_T + K_d) - \sqrt{(M + [RNA]_T + K_d)^2 - (4M[RNA]_T)}] \quad (1)$$

total concentrations of RNA and added metal, respectively, and Δ_{obs} is the observed shift for each data point. Samples prepared by in vitro synthesis contain a 5′-GTP, which has an affinity for Mg^{2+} of ∼19 μM in 0.1 M NaCl (*52*), and so data obtained on these samples were corrected for Mg^{2+}-GTP binding.

Equation 1 assumes a single metal site and that the free metal ion concentration can be calculated from the combination of bound and total metal. As has been pointed out (*34*, *58*), because RNAs may have multiple sites for divalent cations, it is more accurate to set the free metal ion concentration by extensive dialysis against a known metal concentration. In most cases presented here the ^{31}P NMR spectral changes were consistent with a single metal site, but they may not report on all metal sites in the molecule, and so the free ion concentration may be underestimated. Therefore, the K_d values presented here represent upper limits. To show that the values determined by the method above are comparable with those determined by equilibrium dialysis, the CG-WT hairpin was dialyzed against varying concentrations of Mg^{2+} and the change in the chemical shift was plotted against the free Mg^{2+} concentration (set by dialysis) and fit to a 1:1 binding isotherm (*54*). Apparent K_d's of 1.2 ± 0.4 and 1.4 ± 0.4 mM were determined for the A6 and A7 phosphate, respectively, which are slightly lower than the values of 1.8 ± 0.2 and 1.9 ± 0.2 mM reported in Table 1. It is important to note that all K_d's reported here reflect the *apparent* affinities for the metal ion in the presence of 0.1 M NaCl.

RESULTS

The 5′-GAAA-3′ tetraloop hairpin sequences under investigation are shown in Figure 1. The 12-nucleotide hairpins

Table 1: Metal−Tetraloop Affinities Determined by ^{31}P NMR

		K_d (mM) (direction of shift, Δ_{obs})[a,b]	
sample	metal	A7	A6
CG WT	Mg^{2+}	1.8 ± 0.3 (+, 0.6)	1.9 ± 0.2 (+, 0.8)
	Cd^{2+}	0.28 ± 0.02 (+, 1.2)	0.11 ± 0.01 (+, 0.7)
	$Co(NH_3)_6^{3+}$	none	0.36 ± 0.06 (+, 0.6)
CG $A_{6,7,8}$-R_p	Mg^{2+}	none	none
	Cd^{2+}	*c* (−, 1.2)	*c* (+, 0.2)
GU WT	Cd^{2+}	0.34 ± 0.06 (+, 1.1)	0.45 ± 0.02 (+, 0.6)
GU A_7-R_p	Cd^{2+}	0.10 ± 0.03 (−, 1.2)	none
GU A_7-S_p	Cd^{2+}	0.22 ± 0.03 (−, 3.0)	0.16 ± 0.01 (+, 1.4)
GU A_6-S_p	Cd^{2+}	0.12 ± 0.02 (+, 1.0)	0.09 ± 0.02 (+, 0.9)
GU A_6-R_p	Cd^{2+}	0.11 ± 0.02 (+, 0.8)	0.08 ± 0.01 (+, 0.9)
	Mg^{2+}	1.26 ± 0.05 (+, 0.5)	1.01 ± 0.02 (+, 0.5)

[a] K_d and Δ_{obs} were calculated with eq 1. K_d's represent apparent values in 0.1 M NaCl and are upper limits (see Materials and Methods). [b] Direction of the shift is denoted (+) for downfield and (−) for upfield. [c] Data do not fit eq 1.

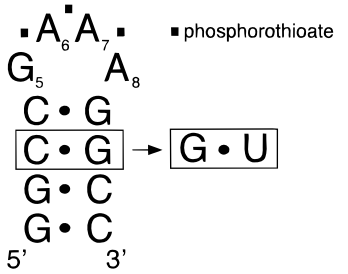

FIGURE 1: The 12-nucleotide 5′-GAAA-3′ hairpin RNA sequences used in this study. The base pair at the 3−10 position is used to designate the hairpin as CG or GU. Phosphorothioate modifications are denoted 5′ to the three adenosine residues.

are designated either "CG" or "GU", depending on the base pair in the 3−10 position of the stem (Figure 1). The GU hairpin sequence was used to facilitate comparison with results described in the accompanying paper, in which the folding thermodynamics of these unmodified and substituted hairpins are reported (*59*).Unmodified hairpins are denoted as wild type (WT), and phosphorothioate modifications are denoted 5′ to the indicated nucleotide as R_p-N or S_p-N. Initially, hairpins with R_p-phosphorothioate modifications introduced 5′ to all three of the loop adenosine residues (R_p-$A_{6,7,8}$) were examined. The effects of single phosphorothioate substitutions were measured using GU hairpins.

^{31}P NMR Analysis of CG-WT GA$_3$ Hairpins. The ^{31}P NMR spectrum of the WT CG hairpin, obtained in 0.1 M NaCl, shows resolved features for all 11 of the phosphodiester bonds (the 5′-triphosphate ^{31}P NMR features are in a different spectral region) (Figure 2). A similar spectrum was reported by Legault and Pardi for this tetraloop sequence, obtained in phosphate buffer and in the absence of NaCl (*33*). On the basis of their assignments, features corresponding to A6 (1.71 ppm), A7 (0.40 ppm), G5 (0.08 ppm), and A8 (−1.25 ppm) in the tetraloop region are indicated in Figure 2.

Upon addition of low concentrations of Mg^{2+} to this sample, shifts are observed in four of the ^{31}P NMR features (Figure 2). Downfield shifts in the A6 and A7 ^{31}P NMR signals are observed, with little additional line broadening. In addition, upfield shifts for the ^{31}P NMR signal corresponding to G5 and an unassigned feature at −0.2 ppm are observed. Shifts in the G5 resonance are accompanied by significant line broadening. These data suggest that Mg^{2+} is binding in a region near the G5, A6, and A7 phosphodiesters.

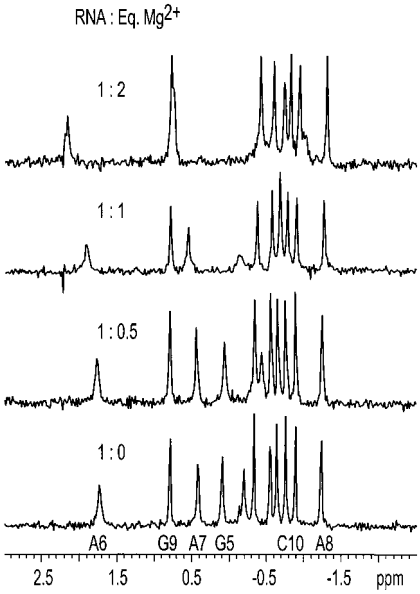

FIGURE 2: Effect of added Mg^{2+} on the ^{31}P NMR spectrum of the 1.57 mM unmodified CG-WT hairpin in the presence of 0, 0.5, 1, and 2 equiv of Mg^{2+}. Spectra were obtained at 121 MHz.

The NMR shifts for these three features were each fit to a simple equilibrium expression assuming binding of a single metal ion to obtain an apparent K_d for Mg^{2+} in 0.1 M NaCl (eq 1 in Materials and Methods). The Mg^{2+}-induced shifts in the A6 and A7 features could be fit with similar apparent dissociation constants of $K_d = 1.8 \pm 0.3$ and 1.9 ± 0.2 mM, respectively (Table 1). Although the feature for G5 moves into the "stem" resonances at higher Mg^{2+} concentrations, a similar value of $K_d \sim 2$ mM was estimated from tentatively assigned peaks. The similarity of K_d's that describe the movement of these three features in the presence of Mg^{2+} suggests that they are all reporting on the same metal interaction with a $K_d \sim 2$ mM for Mg^{2+} in 0.1 M NaCl. This study was conducted at two different RNA concentrations, 1.5 and 0.36 mM, and similar dissociation constants of ∼2 mM are obtained in both cases (data not shown). As noted in Materials and Methods, the apparent K_d's represent upper limits.

The ammine ligands of $Co(NH_3)_6^{3+}$ are exchange-inert, thus making $Co(NH_3)_6^{3+}$ a useful probe for inner- vs outer-sphere (i.e., through water) metal−RNA interactions (*26*, *58*, *60*). Addition of $Co(NH_3)_6^{3+}$ to WT-CG RNA results in a downfield shift of the A6 ^{31}P NMR signal and some shifts in features from the hairpin stem (Figure S1; see paragraph at end of paper regarding Supporting Information). Resonances for the A7 and G5 phosphates are not perturbed, however, even by addition of up to 10 equiv of $Co(NH_3)_6^{3+}$. The total downfield shift of the A6 ^{31}P NMR signal is 0.6 ppm in the presence of $Co(NH_3)_6^{3+}$ ($K_d = 0.36$ mM), compared to 0.8 ppm with addition of Mg^{2+}.

Mg^{2+}−phosphate interactions are generally characterized by a downfield ^{31}P NMR shift that is consistent with deshielding of the phosphorus nucleus (*51*, *52*). The Mg^{2+}-induced downfield shifts of the ^{31}P NMR signals for A6 and A7 in the WT-CG hairpin suggest that the metal is directly coordinating to one or both of these phosphates. The upfield shifts of the G5 phosphodiester feature and the unassigned peak at −0.2 ppm suggest that other effects such as metal-induced conformational changes are affecting these sites. The

NMR data obtained in the presence of $Co(NH_3)_6^{3+}$ indicate that this ion has no effect on the A7 phosphodiester and also does not result in the upfield shift of the G5 phosphodiester. These results are consistent with a model in which there is an inner-sphere Mg^{2+}−A7 phosphate interaction that cannot be satisfied by $Co(NH_3)_6^{3+}$. The upfield shift in the ^{31}P NMR signal of G5 that accompanies Mg^{2+} binding may be due to a change in this phosphodiester bond geometry.

In the experiments described below with phosphorothioate-modified samples, Cd^{2+} was used as a probe for sites whose sulfur modification may create a diminished affinity for Mg^{2+}. Titration of the unmodified WT-CG hairpin with Cd^{2+} (data not shown) induced downfield shifts in A6 and A7 as observed with Mg^{2+}, with lower K_d's indicating ~10 times higher affinity for this ion (Table 1). For Cd^{2+}, the G5 feature shifts downfield rather than showing the distinct upfield shift observed in the presence of Mg^{2+}. The binding mode of Cd^{2+} thus still involves the A6 and A7 sites but is different from that of Mg^{2+} in its effect at G5.

^{31}P NMR Analysis of GA_3 Hairpins with Phosphorothioate Modifications. Phosphorothioate modifications were investigated to provide further insight into the location and ion specificity of the metal−GA_3 hairpin interactions. Phosphorothioate modifications allow sulfur substitution of either the *pro-R* or the *pro-S* position of the phosphodiester and provide a probe for metal specificity. If the site interaction involves a direct "inner-sphere" metal−phosphate interaction, the "softer" sulfur ligand should discriminate between Mg^{2+} and the more thiophilic Cd^{2+}. An outer-sphere, through-water interaction may not result in a strong metal ion specificity in the phosphorothioate-substituted samples.

Previous work has reported upfield shifts in ^{31}P NMR features from phosphorothioates upon binding Cd^{2+}. This has been observed for phosphorothioate-substituted adenine and guanine nucleotides (*51, 52*), as well as the simple compound diethylthiophosphate (*61*), and is in contrast to the downfield ^{31}P NMR shifts reported upon binding Mg^{2+} or Cd^{2+} to unsubstituted phosphodiester groups. Thus, in the case of an inner-sphere metal−phosphate interaction, the direction of the metal-induced ^{31}P NMR shift is expected to change upon substitution with a phosphorothioate.

In vitro synthesis of the CG hairpin using ATPαS introduced three R_p-phosphorothioates (R_p-$A_{6,7,8}$) and provided a ^{31}P NMR spectrum that exhibits three downfield-shifted peaks, assigned on the basis of individual R_p substitutions (see below) as A7 (60.4 ppm), A6 (59.8 ppm), and A8 (57.2 ppm) (Figure S2). Addition of Mg^{2+} has little effect on these three ^{31}P NMR signals. Upon addition of 5 equiv of Cd^{2+}, however, a total upfield shift of 1.2 ppm in the A7 ^{31}P NMR resonance is observed (Figure S2). This Cd^{2+}-induced upfield shift of the A7 feature in the sulfur-substituted sample and the Mg^{2+}-induced downfield shift for this feature in the WT sample suggest that a metal is binding specifically to the A7 phosphate/phosphorothioate in the tetraloop.

^{31}P NMR Analysis of GU Hairpins with Single Phosphorothioate Modifications. The accompanying paper describes thermal denaturation studies of 5′-GAAA-3′ hairpins with either the CG or GU wobble base pair in the stem (Figure 1). The GU hairpins were used to explore the thermodynamic impact of individual phosphorothioate modifications due to favorable optical melting profiles (lower t_m's in comparison with the CG hairpins). It was found that a single R_p-phosphorothioate modification 5′ to A7 results in a surprising increase in t_m that is not observed in any other singly substituted hairpin (*59*). An increase in t_m also is observed in the R_p-$A_{6,7,8}$-substituted hairpins for both the CG and the GU sequences. The distinctive behavior for these hairpins suggests a difference in structure caused by an R_p-phosphorothioate substitution at the A7 site.

^{31}P NMR data were collected for WT-GU hairpins (data not shown) and samples with single R_p and S_p substitutions (Figures 3 and 4), as well as for the multiply substituted GU-R_p-$A_{6,7,8}$ hairpin (data not shown). Although a full ^{31}P assignment of the 1-D ^{31}P spectrum for this hairpin is not available, features for the A6, A7, and A8 positions in the tetraloop appear in expected positions and shift with addition of Mg^{2+} and Cd^{2+}, as found for the CG hairpin sample (Table 1). Because the A8 phosphodiester shows no metal interactions, only the A7- and A6-substituted samples are described below.

The effects of Cd^{2+} on the GU hairpins with R_p and S_p sulfur substitutions at both A6 and A7 are shown in Figure 3. Both the R_p-A7 and S_p-A7 hairpins show an upfield shift of the A7 ^{31}P NMR resonance upon addition of Cd^{2+} (Figure 3, right). The upfield shifts are consistent with coordination of Cd^{2+} to the A7 phosphorothioate in both diastereomers, although as noted above the R_p-A7 sample may have a unique structure. In contrast, both R_p-A6 and S_p-A6 hairpins exhibit a *downfield* shift in the A6 resonance upon addition of Cd^{2+} (Figure 3, left). On the basis of previous studies of Cd^{2+}-phosphorothioates, the downfield shift of the A6 phosphorothioate feature with added Cd^{2+} is inconsistent with direct metal ion coordination to the phosphorothioate being the only effect contributing to the change in the spectra. Taken together, these data support a model in which the metal ion is binding via direct coordination at the A7 position and influences the A6 phosphate possibly via an outer-sphere interaction or by a conformational change.

The features in the 2 to −2 ppm region of the ^{31}P NMR spectra corresponding to the unmodified phosphodiester bonds provide additional information about these phosphorothioate-substituted samples. In this region the GU hairpin ^{31}P NMR spectra (Figure 4) are less resolved than those of the CG hairpin (Figure 2), exhibiting several overlapping features. The ^{31}P NMR spectra of both GU-R_p-A6 and GU-S_p-A6 are similar in this region (Figure 4A,B). For substitutions at A7, the two isomers yield ^{31}P NMR spectra that differ (Figure 4C,D). Interestingly, the ^{31}P NMR spectrum in this unmodified region is distinctive for the GU-R_p-A7 hairpin, showing 10 well-resolved features (Figure 4D). In the accompanying paper, optically detected thermal denaturation data are presented that show this GU-R_p-A7 isomer to be dramatically stabilized [$\Delta(\Delta G_{37°C}) \sim -3$ kcal mol^{-1}] over the other singly phosphorothioate-substituted hairpins, including the S_p-A7 isomer (*59*). The ^{31}P NMR spectra in Figure 4 also reflect a different conformation for the stabilized R_p-A7 hairpin, the structural details of which are currently being pursued. Added Cd^{2+} produces little to no change in the unmodified region of the ^{31}P NMR spectra for the R_p-A7 hairpin, making it distinctive from the R_p-A6, S_p-A6, and S_p-A7 hairpins for which the unmodified region of the ^{31}P NMR spectra show changes similar to those observed in WT hairpin (data not shown). This again

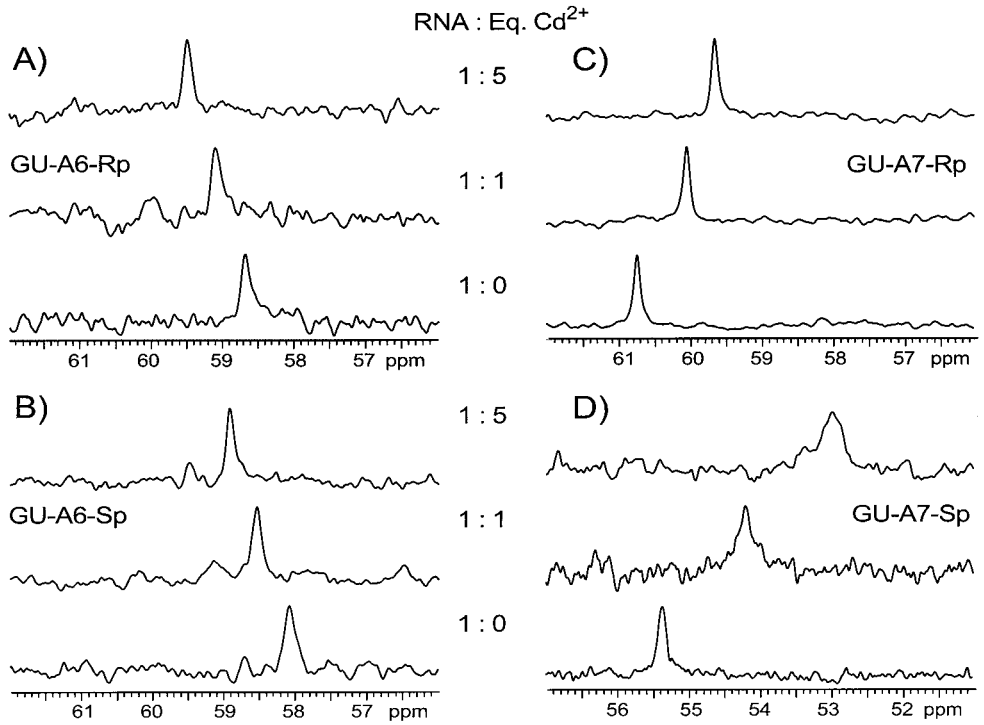

FIGURE 3: Effect of added Cd^{2+} on the ^{31}P NMR spectra of GU hairpins containing single phosphorothioate modifications. ^{31}P NMR spectra of (A) 0.16 mM GU-R_p-A6 RNA, (B) 0.16 mM GU-S_p-A6 RNA, (C) 0.4 mM GU-R_p-A7 RNA, and (D) 0.21 mM GU-S_p-A7 RNA with 0, 1, and 5 equiv of added Cd^{2+}. Spectra in (A), (B), and (D) were obtained at 202 MHz, and those in (C) were obtained at 121 MHz.

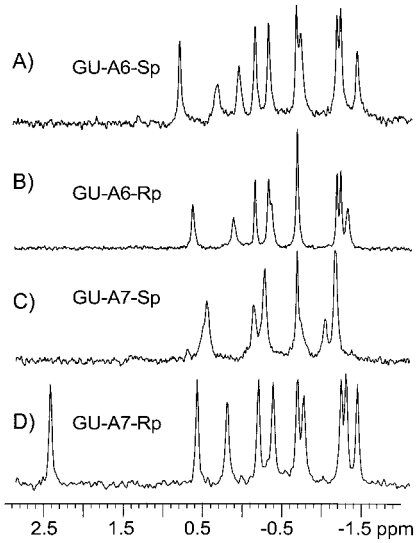

FIGURE 4: Comparison of the ^{31}P NMR spectral region due to unmodified phosphodiesters of the GU hairpins containing single phosphorothioate modifications. ^{31}P NMR spectra of (A) 0.16 mM GU-S_p-A6 RNA, (B) 0.16 mM GU-R_p-A6 RNA, (C) 0.21 mM GU-S_p-A7 RNA, and (D) 0.4 mM GU-R_p-A7 RNA. Spectra in (A), (B), and (C) were obtained at 202 MHz, and that in (D) was obtained at 121 MHz.

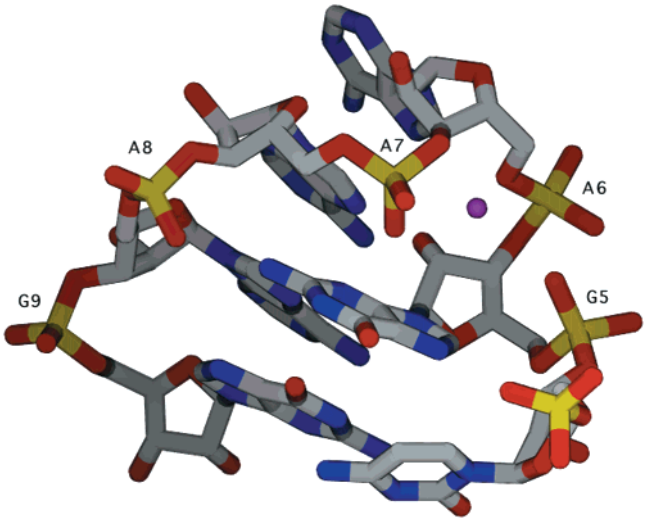

FIGURE 5: Molecular model of nucleotides C4−G9 of the 5′-GAAA-3′ hairpin with a $Mg(OH_2)_5^{2+}$ directly coordinated to the *pro-S* oxygen of A7 (water molecules are not shown in the structure). Molecular dynamics simulations were done using the Universal Forcefield in Cerius. Initial RNA coordinates were taken from Jucker et al. (PDB 1ZIF) (*25*). The movement of the RNA was restricted, with the exception of the phosphates at G5, A6, and A7. A total of 50 000 steps of quench dynamics followed minimization to give the resulting structure.

indicates that the structure of the R_p-A7 hairpin is different from those of the other phosphorothioate-substituted samples examined here.

DISCUSSION

The ^{31}P NMR spectra presented here show shifts demonstrating localized metal interactions in the GAAA tetraloop region of the RNA hairpins in Figure 1. To aid in discriminating between ^{31}P NMR shifts due to direct metal binding and shifts induced by conformational changes or other effects, we have compared unsubstituted hairpins with samples having single phosphorothioate substitutions. The use of thiophilic Cd^{2+}, nonthiophilic Mg^{2+}, and exchange-inert $Co(NH_3)_6^{3+}$ in combination with these substitutions provides information that can be used to predict the coordination environment of this metal site. These predictions have been used in conjunction with reported structural coordinates and molecular dynamics simulations to construct a model for the metal−tetraloop interaction (Figure 5).

An important assumption that is often made in using phosphorothioate substitutions to detect metal-binding effects is that the sulfur substitution does not affect the global structure of the RNA molecule. In the GA_3 hairpins examined here by NMR and in the accompanying paper by thermal denaturation experiments, we find that one out of six possible diastereomeric phosphorothioate substitutions 5′ to adenosines in the GA_3 loop causes an apparent structural change in the RNA, as evidenced by an increase in t_m and a marked change in the ^{31}P NMR spectra. The nature of this structural change caused by the R_p-A7 substitution is under current investigation. One possibility is that a monomer−dimer equilibrium is influenced by this substitution, such that the R_p-A7 samples are more stable as duplexes with an internal bulge. Previous attempts to crystallize small-sequence models for tetraloops have resulted in formation of such duplexes (*62*). Duplex formation should result in a concentration dependence of the measured t_m, and no such increase was observed in thermal denaturation studies of R_p-A7 hairpins carried out over the concentration range of 1−30 μM (*59*). At this time, we cannot, however, rule out duplex formation at the higher ($\geq$100 μM) concentrations used in these NMR experiments. Because of the apparent structural difference in the R_p-A7 sample, we do not include it in the discussion below in hypothesizing a model for the metal-binding site in GA_3 tetraloops.

In unsubstituted GA_3 hairpin samples, addition of Mg^{2+} causes downfield shifts in ^{31}P NMR features assigned to A7 and A6 and upfield shifts in the feature assigned to G5. These shifts are assigned to a single site on the basis of similar apparent K_d's of ~2 mM for Mg^{2+} (0.1 M NaCl). $Co(NH_3)_6^{3+}$ only affected A6, and to a lesser extent, suggesting that an inner-sphere metal ion coordination contributes to the Mg^{2+}-induced shifts in A7 and G5. The ^{31}P NMR features from single phosphorothioate substitutions at A6 and A7 showed very different effects upon addition of thiophilic Cd^{2+}. Unlike Mg^{2+}− and Cd^{2+}−phosphate interactions, Cd^{2+}−thiophosphate interactions have been observed to cause an upfield shift in the ^{31}P NMR spectrum of the coordinating phosphate, and so the upfield shift observed in the S_p-A7 tetraloop is consistent with direct metal−phosphate interactions at the A7 site. By contrast, both R_p- and S_p-A6 phosphorothioates exhibit downfield ^{31}P NMR shifts upon addition of Cd^{2+}. In sum, from these data we predict that the GA_3 tetraloop metal site consists of inner-sphere phosphodiester coordination at A7, accompanied possibly by outer-sphere phosphodiester coordination or conformational changes at A6 and G5.

The model of a metal site consisting of inner-sphere coordination at A7 and outer-sphere or other effects at A6 would predict that phosphorothioate substitution at A6 would not perturb interaction of Mg^{2+} with the A7 phosphodiester. This in turn predicts that addition of Mg^{2+} to the A6-phosphorothioate-substituted samples will cause downfield shifts in both A6 (modified) and A7 (unmodified) features, with affinities similar to those observed for Mg^{2+} in the WT sample. As predicted, this is the result observed for both the R_p-A6 and S_p-A6 GU hairpins with addition of Mg^{2+} (Table 1). The Mg^{2+} affinity calculated from shifts of the A6 and A7 ^{31}P NMR features in the R_p-A6 RNA sample of K_d ~1.1 mM is very similar to the wild-type, unsubstituted sample.

Several structures are available for GAAA tetraloops, providing a basis with which to model this putative metal site. Using coordinates from the NMR-derived structure published by Jucker and co-workers (*25*), a Mg^{2+} ion was placed directly coordinated to the A7 phosphate, and the structure was minimized using restrained molecular dynamics simulations. The resulting model is shown in Figure 5. To create this model, the Mg^{2+} was coordinated directly to the *pro-S* oxygen of the A7 phosphate, with five water molecules completing the coordination sphere. The structure was restricted with the exception of the G5, A6, and A7 phosphodiester bonds, and these dihedral angles were compared before and after energy minimization of the structure. The Mg^{2+} ion fits nicely into a pocket created by the close approach of the A7 and A6 phosphates, an area that also shows a relatively negative electrostatic potential in GRASP-type structures depicting the electrostatic surface of the molecule (data not shown).[2] After energy minimization in the presence of the metal ion, the dihedral angles α and ζ of the phosphodiester 5′ to A6 change by 23° and 15°, respectively, whereas the corresponding change at A7 is only 7° and 4°. Gorenstein and co-workers have simulated phosphodiester ^{31}P chemical shift changes as a function of dihedral angle (*64*), which indicate that the angle changes predicted for A6 by this model would be accompanied by a chemical shift change of $\geq$0.4 ppm, similar to that observed here in the A6 ^{31}P NMR feature with addition of metals. The G5 phosphate dihedral angles, however, did not change significantly following energy minimization (9° and 7°). This contrasts with predictions based on the ^{31}P NMR spectra and may reflect the restrictions in these simple calculations, which did not include movement of the base or sugar moieties. Of note, published X-ray crystal structures of GNRA tetraloops have not reported sites occupied by metal ions, which may be due to competition with monovalent cations from the high ionic strength in the crystallizing buffers.

Few studies have provided structural information and affinities for metal sites in RNA under solution conditions. Tinoco and co-workers have characterized a metal−RNA interaction in the stem of a GNRA tetraloop model through observation of NOE's between the RNA and the ammine protons of $Co(NH_3)_6^{3+}$ (*26*). This metal site is localized to a pair of G·U base pairs beneath the loop region of the tetraloop model with hydrogen bonding predicted between the ammine ligands and bases in the major groove of the stem region. The tetraloops investigated here do not contain the repeating G·U base pairs, and in this case, Mg^{2+} appears to interact at the loop sites with the highest affinity, although ^{31}P features from the stems are perturbed with $Co(NH_3)_6^{3+}$. Metal interactions in the junction regions of RNA pseudoknots also have been characterized thermodynamically and by solution ^{1}H NMR in the presence of $Co(NH_3)_6^{3+}$ (*58*, *65*). In the above cases, the metal interaction has been characterized as a delocalized, nonspecific electrostatic attraction to a region of relatively high negative charge density in the RNA. In a very recent report, Rüdisser and Tinoco observed NOE cross-peaks between protons in the tetraloop region of

[2] An electrostatic surface plot generated using the coordinates from Pley et al. (*28*), using the program SPOCK with potentials of −5 to −26 kT/e, shows a relatively higher negative charge in the area near the GA_3 tetraloop of stem II of the hammerhead ribozyme. Chin et al. (*63*) recently reported no pockets of negative potential for a GA_3 tetraloop in the P456 core of the group I intron; however, the potentials used were over a larger range from −5 to −100 kT/e.

a GA_3 tetraloop and the ammine ligands of $Co(NH_3)_6^{3+}$, predicting a metal-binding pocket similar to the one reported here (*36*). By monitoring the change in the chemical shift of the imino proton of G5 with added Mg^{2+} and $Co(NH_3)_6^{3+}$, the authors measured upper limits for the binding affinities of these ions of $K_d = 2$ (±1) and 7 (±5) mM, respectively, and predicted an inner-sphere Mg^{2+}−phosphate interaction on the basis of those relative affinities. A similar affinity of $K_d \sim 2$ mM (Mg^{2+}, 0.1 M NaCl) is measured for the tetraloop site observed here, placing this in the class of relatively weak metal−RNA interactions and similar in magnitude to affinities measured for nonspecific metal−phosphate interactions in ribooligonucleotides. Although the measured affinity for Mg^{2+} is not high, the ^{31}P NMR data presented here support a localized site with apparent inner-sphere metal−phosphate character. More extensive structural studies should aid in clarifying if other conformational changes are caused by this metal interaction.

SUPPORTING INFORMATION AVAILABLE

Figure S1 showing the effect of added (A) Mg^{2+} and (B) $Co(NH_3)_6^{3+}$ on the 121 MHz ^{31}P NMR spectrum of the CG-WT hairpin and Figure S2 showing the effect of added Cd^{2+} on the 121 MHz ^{31}P NMR spectrum of a phosphorothioate-modified CG hairpin (CG-R_p-$A_{6,7,8}$ RNA). This information is available free of charge via the Internet at http://pubs.acs.org.

REFERENCES

1. Michel, F., and Westhof, E. (1990) *J. Mol. Biol. 216*, 585−610.
2. Woese, C. R., Winker, S., and Gutell, R. R. (1990) *Proc. Natl. Acad. Sci. U.S.A. 87*, 8467−8471.
3. Tuerk, C., Gauss, P., Thermes, C., Groebe, D. R., Gayle, M., Guild, N., Stormo, G., D'Aubenton-Carafa, Y., Uhlenbeck, O. C., Tinoco, I., Jr., Brody, E. N., and Gold, L. (1988) *Proc. Natl. Acad. Sci. U.S.A. 85*, 1364−1368.
4. Antao, V. P., Lai, S. Y., and Tinoco, I., Jr. (1991) *Nucleic Acids Res. 19*, 5901−5905.
5. Antao, V. P., and Tinoco, I., Jr. (1992) *Nucleic Acids Res. 20*, 819−824.
6. Santa Lucia, J., Kierzek, R., and Turner, D. H. (1992) *Science 256*, 217−219.
7. Uhlenbeck, O. C. (1990) *Nature 346*, 613−614.
8. Cate, J. H., Gooding, A. R., Podell, E., Zhou, K., Golden, B. L., Kundrot, C. E., Cech, T. R., and Doudna, J. A. (1996) *Science 273*, 1678−1685.
9. Costa, M., and Michel, F. (1995) *EMBO J. 14*, 1276−1285.
10. Jaeger, L., Michel, F., and Westhof, E. (1994) *J. Mol. Biol. 236*, 1271−1276.
11. Murphy, F. L., and Cech, T. R. (1994) *J. Mol. Biol. 236*, 49−63.
12. Pley, H. W., Flaherty, K. M., and McKay, D. B. (1994) *Nature 372*, 111−113.
13. Abramovitz, D. L., and Pyle, A. M. (1997) *J. Mol. Biol. 266*, 493−506.
14. Gluck, A., Endo, Y., and Wool, I. G. (1992) *J. Mol. Biol. 226*, 411−424.
15. Gluck, A., Endo, Y., and Wool, I. G. (1994) *Nucleic Acids Res. 22*, 321−324.
16. Allen, P., Worland, S., and Gold, L. (1995) *Virology 209*, 327−336.
17. Perbandt, M., Nolte, A., Lorenz, S., Bald, R., Betzel, C., and Erdmann, V. A. (1998) *FEBS Lett. 429*, 211−215.
18. Legault, P., Li, J., Mogridge, J., Kay, L. E., and Greenblatt, J. (1998) *Cell 93*, 289−299.
19. Chanfreau, G., and Jacquier, A. (1996) *EMBO J. 15*, 3466−3476.
20. Konforti, B. B., Liu, Q., and Pyle, A. M. (1998) *EMBO J. 17*, 7105−7117.
21. Orita, M., Nishikawa, F., Shimayama, T., Taira, K., Endo, Y., and Nishikawa, S. (1993) *Nucleic Acids Res. 21*, 5670−5678.
22. Szewczak, A. A., Moore, P. B., Chan, Y.-L., and Wool, I. G. (1993) *Proc. Natl. Acad. Sci. U.S.A. 90*, 9581−9585.
23. Cheong, C., Varani, G., and Tinoco, I., Jr. (1990) *Nature 346*, 680−682.
24. Heus, H. A., and Pardi, A. (1991) *Science 253*, 191−194.
25. Jucker, F. M., Heus, H. A., Yip, P. F., Moors, E. H. M., and Pardi, A. (1996) *J. Mol. Biol. 264*, 968−980.
26. Kieft, J. S., and Tinoco, I., Jr. (1997) *Structure 5*, 713−721.
27. Shen, L. X., Cai, Z., and Tinoco, I., Jr. (1995) *FASEB J. 9*, 1023−1033.
28. Pley, H. W., Flaherty, K. M., and McKay, D. B. (1994) *Nature 372*, 68−74.
29. Scott, W. G., Finch, J. T., and Klug, A. (1995) *Cell 81*, 991−1002.
30. Scott, W. G., Murray, J. B., Arnold, J. R. P., Stoddard, B. L., and Klug, A. (1996) *Science 274*, 2065−2069.
31. Correll, C. C., Munishkin, A., Chan, Y.-L., Ren, Z., Wool, I. G., and Steitz, T. A. (1998) *Proc. Natl. Acad. Sci. U.S.A. 95*, 13436−13441.
32. Stallings, S. C., and Moore, P. B. (1997) *Structure 5*, 1173−1185.
33. Legault, P., and Pardi, A. (1994) *J. Magn. Reson., Ser. B 103*, 82−86.
34. Hansen, M. R., Simorre, J. P., Hanson, P., Mokler, V., Bellon, L., Beigelman, L., and Pardi, A. (1999) *RNA 5*, 1099−1104.
35. Hunsicker, L., and DeRose, V. J., unpublished results.
36. Rüdisser, S., and Tinoco, I., Jr. (2000) *J. Mol. Biol. 295*, 1211−1223.
37. Ruffner, D. E., and Uhlenbeck, O. C. (1990) *Nucleic Acids Res. 18*, 6025−6029.
38. Slim, G., and Gait, M. J. (1991) *Nucleic Acids Res. 19*, 1183−1188.
39. Dahm, S. C., and Uhlenbeck, O. C. (1991) *Biochemistry 30*, 9464−9469.
40. Koizumi, M., and Ohtsuka, E. (1991) *Biochemistry 30*, 5145−5150.
41. Zhou, D.-M., Kumar, P. K. R., Zhang, L.-H., and Taira, K. (1996) *J. Am. Chem. Soc. 118*, 8969−8970.
42. Knoll, R., Bald, R., and Furste, J. P. (1997) *RNA 3*, 132−140.
43. Peracchi, A., Beigelman, L., Scott, E. C., Uhlenbeck, O. C., and Herschlag, D. (1997) *J. Biol. Chem. 272*, 26822−26826.
44. Scott, E. C., and Uhlenceck, O. C. (1999) *Nucleic Acids Res. 27*, 479−484.
45. Sood, V. D., Beattie, T. L., and Collins, R. A. (1998) *J. Mol. Biol. 282*, 741−750.
46. Christian, E. L., and Yarus, M. (1992) *J. Mol. Biol. 228*, 743−758.
47. Christian, E. L., and Yarus, M. (1993) *Biochemistry 32*, 4475−4480.
48. Boudvillain, M., and Pyle, A. M. (1998) *EMBO J. 17*, 7091−7104.
49. Eckstein, F. (1985) *Annu. Rev. Biochem. 54*, 367−402.
50. Sheu, K. R., and Frey, P. A. (1977) *J. Biol. Chem. 252*, 4445−4448.
51. Jaffe, E. K., and Cohn, M. (1978) *Biochemistry 17*, 652−657.
52. Pecoraro, V. L., Hermes, J. D., and Cleland, W. W. (1984) *Biochemistry 23*, 5262−5271.
53. Milligan, J. F., Groebe, D. R., Witherell, G. W., and Uhlenbeck, O. C. (1987) *Nucleic Acids Res. 15*, 8783−8798.
54. Horton, T. E., Clardy, D. R., and DeRose, V. J. (1998) *Biochemistry 37*, 18094−18101.
55. Warshaw, M. M., and Tinoco, I., Jr. (1966) *J. Mol. Biol. 20*, 29−38.
56. Griffiths, A. D., Potter, B. V. L., and Eperon, I. C. (1987) *Nucleic Acids Res. 15*, 4145−4162.
57. Eckstein, F., and Goody, R. S. (1976) *Biochemistry 15*, 1685−1691.
58. Gonzalez, R. L., and Tinoco, I., Jr. (1999) *J. Mol. Biol. 289*, 1267−1282.

59. Horton, T. E., Maderia, M., and DeRose, V. J. (2000) *Biochemistry 39*, 8201−8207.
60. Cowan, J. A. (1993) *J. Inorg. Biochem. 49*, 171−175.
61. Maderia, M., and DeRose, V. J., unpublished results.
62. Baeyens, K. J., De Bondt, H. L., Pardi, A., and Holbrook, S. R. (1996) *Proc. Natl. Acad. Sci. U.S.A. 93*, 12851−12855.
63. Chin, K., Sharp, K. A., Honig, B., and Pyle, A. M. (1999) *Nat. Struct. Biol. 6*, 1055−1061.
64. Gorenstein, D. G., Ed. (1984) *Phosphorous-31 NMR, Principles and Applications*, Academic Press, Orlando, FL.
65. Nixon, P. L., Theimer, C. A., and Giedroc, D. P. (1999) *Biopolymers 50*, 443−458.

BI000140L